

Quantum molecular dynamics study of warm dense ironCong Wang,^{1,2} Zhe-Bin Wang,³ Qi-Feng Chen,⁴ and Ping Zhang^{1,2,*}¹*Institute of Applied Physics and Computational Mathematics, P.O. Box 8009, Beijing 100088, People's Republic of China*²*Center for Applied Physics and Technology, Peking University, Beijing 100871, People's Republic of China*³*Research Center of Laser Fusion, China Academy of Engineering Physics, Mianyang 621900, People's Republic of China*⁴*Institute of Fluid Physics, China Academy of Engineering Physics, Mianyang 621900, People's Republic of China*

(Received 28 October 2013; published 6 February 2014)

The equation of state, the self-diffusion coefficient and viscosity of fluid iron in the warm dense regime at densities from 12.5 to 25.0 g/cm³, and temperatures from 0.5 to 15.0 eV have been calculated via quantum molecular dynamics simulations. The principal Hugoniot is in good agreement with nuclear explosive experiments up to ~50 Mbar but predicts lower pressures compared with high intensity laser results. The self-diffusion coefficient and viscosity have been simulated and have been compared with the one-component plasma model. The Stokes-Einstein relationship, defined by connections between the viscosity and the self-diffusion coefficient, has been determined and has been found to be fairly well described by classical predictions.

DOI: [10.1103/PhysRevE.89.023101](https://doi.org/10.1103/PhysRevE.89.023101)

PACS number(s): 52.25.Fi, 64.30.-t, 66.20.-d, 51.30.+i

I. INTRODUCTION

Due to technological, geological, and sociological importance, iron is one of the most studied materials. The demands for models of materials in the warm dense regime is of great interest in the context of astrophysics [1] and other fields of applications, such as the inertial confinement fusion, the realization of x-ray sources, and the interpretation of XUV spectroscopy experiments [2–4]. Accurate knowledge of the thermophysical properties of iron at the warm dense matter (WDM) regime, such as the equation of state (EOS), transport properties, and opacity [5], is essential in constructing a realistic model of Earth and in the description of the transition between the liquid outer core and the solid inner core [6,7] where pressure between 1.3 and 3.7 Mbar is reached. The behavior of iron at pressures higher than that reached inside the Earth is of concern to many fields. For instance, the nature of the continuous transition from condensed matter to dense plasma is an outstanding and interesting issue in high-pressure physics [8], featuring pressures in the 1–50 Mbar range. Iron has been found in the rocky cores of intermediate planets with masses bigger than the Earth, such as Uranus and Neptune [9], where the internal pressure exceeds 3.7 Mbar. Since the problems of opacity and the EOS were addressed, the interest in this field has remained constant, and more experimental detections combined with theoretical approaches have appeared.

The EOS of iron at pressures above a few megabars can be detected by dynamical methods, such as two-stage light-gas guns [10], chemical [11] or nuclear explosions [12–20], and high intensity laser driven experiments [21]. However, there only exists a total of 18 EOS points above 10 Mbar as reported in the scientific literature for iron at the normal initial density. Possibly, due to the lack of EOS data, some models indicate rather different high-pressure behaviors. For instance, the compressibility of iron at 40 Mbar is ~2.7 as predicted by the well known quotidian equation of state model [22], and the results are substantially smaller than that

of the SESAME table [23]. Theoretical papers have been devoted to the EOS of warm dense iron in a wide range by using Thomas-Fermi (TF) molecular dynamics (MD) and average-atom models [24–26]. Recently, the quantum molecular dynamics (QMD) method [27], where the quantum-mechanical treatments combining classical molecular dynamics for ions and finite-temperature density functional theory (FT-DFT) for electrons, proved suitable for modeling WDM.

In this paper, we have selected iron as a representative system and have examined the EOS and transport properties (viscosity and self-diffusion coefficient) in the warm dense regime that covers the standard extreme condition as reached in the interior of Earth and in shock wave experiments. The thermophysical properties of the species have been derived from QMD simulations. In the next section, we present the formalism for QMD and for determining the static and transport properties. Then, EOS, viscosity, and diffusion coefficients for iron are presented, and the QMD results are compared with the results from reduced models. Finally, concluding remarks are given.

II. FORMALISM

Brief descriptions of the fundamental formalism used to simulate fluid iron are presented; please find details elsewhere as indicated in Ref. [28]. The basic quantum-mechanical DFT forms the basis of our calculations. Numerical schemes for determining diffusion and viscosity are presented.

A. Quantum molecular dynamics

QMD simulations have been applied to study warm dense iron by using the Vienna *ab initio* simulation package [29,30]. In the present paper, electrons are treated fully quantum mechanically by employing a plane-wave FT-DFT local spin density approximation where the electronic states follow from the Fermi-Dirac distribution. The ions move classically according to the forces from the electron density and the ion-ion repulsion. The electron wave functions are calculated with the projector augmented wave potential. Simulations have been performed in the *NVT* (canonical) ensemble where the

*Corresponding author: zhang_ping@iapcm.ac.cn

number of particles N and the volume are fixed. The system was assumed to be in local thermodynamic equilibrium with the electron and ion temperatures being equal ($T_e = T_i$). In these calculations, the electronic temperature has been kept constant according to the Fermi-Dirac distribution, and the ion temperature is controlled by the No se thermostat [31].

At each step during the MD simulations, a set of electronic state functions $[\Psi_{i,k}(r,t)]$ for each \mathbf{k} point is determined within the Kohn-Sham construction by

$$H_{\text{KS}}\Psi_{i,k}(r,t) = \epsilon_{i,k}\Psi_{i,k}(r,t), \quad (1)$$

with

$$H_{\text{KS}} = -\frac{1}{2}\nabla^2 + V_{\text{ext}} + \int \frac{n(r')}{|r-r'|}dr' + v_{\text{xc}}(r), \quad (2)$$

in which the four terms, respectively, represent the kinetic contribution, the electron-ion interaction, the Hartree contribution, and the exchange-correlation term. The electronic density is obtained by

$$n(r) = \sum_{i,k} f_{i,k} |\Psi_{i,k}(r,t)|^2. \quad (3)$$

Then by applying the velocity Verlet algorithm, based on the force from interactions between ions and electrons, a new set of positions and velocities is obtained for the ions.

All simulations are performed with 128 atoms for fluid iron where a cubic supercell of length L (volume $V = L^3$) is periodically repeated. The simulated densities range from 12.5 to 25.0 g/cm³. The temperature range from 0.5 to 15 eV has been selected to highlight the conditions as reached in nuclear explosion and high power laser experiments. The convergence of the thermodynamic quantities has been checked in the present paper, and a plane-wave cutoff energy of 600 eV is employed in all simulations so that the pressure is converged within 2%. We have also checked out the convergence with respect to a systematic enlargement of the \mathbf{k} -point set in the representation of the Brillouin zone. The correction of higher-order \mathbf{k} points in the EOS data is slight and negligible. In the molecular dynamics simulations, only the Γ point of the Brillouin zone is included. The dynamic simulation lasts for 20 000 steps with time steps of 1–4 fs according to different densities and temperatures. For each pressure and temperature, the system is equilibrated within 0.5–1 ps. The EOS data are obtained by averaging over the final 1–3 ps molecular dynamics simulations.

B. Transport properties

The self-diffusion coefficient D can either be calculated from the trajectory by the mean-square displacement,

$$D = \frac{1}{6t} \langle |R_i(t) - R_i(0)|^2 \rangle, \quad (4)$$

or be calculated by the velocity autocorrelation function,

$$D = \frac{1}{3} \int_0^\infty \langle V_i(t)V_i(0) \rangle dt, \quad (5)$$

where R_i is the position and V_i is the velocity of the i th nucleus. Only in the long-time limit are these two formulas of D formally equivalent. Sufficient lengths of the trajectories

have been generated to secure contributions from the velocity autocorrelation function so the quadrature vanishes, and the mean mean-square displacement away from the origin consistently fits to a straight line. The diffusion coefficients obtained from these two approaches lie within 1% accuracy of each other. Here, we report the results for the velocity.

The viscosity,

$$\eta = \lim_{t \rightarrow \infty} \bar{\eta}(t) \quad (6)$$

has been computed from the autocorrelation function of the off-diagonal component of the stress tensor [32],

$$\bar{\eta}(t) = \frac{V}{k_B T} \int_0^t \langle P_{12}(0)P_{12}(t') \rangle dt'. \quad (7)$$

The results are averaged from the five independent off-diagonal components of the stress tensor P_{xy} , P_{yz} , P_{zx} , $(P_{xx} - P_{yy})/2$, and $(P_{yy} - P_{zz})/2$.

Different from the self-diffusion coefficient, which involves single-particle correlations and reaches significant statistical improvement upon averaging over the particles, the viscosity depends on the entire system and, thus, needs very long trajectories so as to gain statistical accuracy. To shorten the length of the trajectory, we use empirical fits [33] to the integrals of the autocorrelation functions. Thus, extrapolation of the fits to $t \rightarrow \infty$ can more effectively determine the basic dynamical properties. Both D and $\bar{\eta}$ have been fit to the functional in the form of $A[1 - \exp(-t/\tau)]$, where A and τ are free parameters. Reasonable approximation to the viscosity can be produced from the finite time fitting procedure, which also serves to damp the long-time fluctuations.

The fractional statistical error in calculating a correlation function C for molecular dynamics trajectories [34] can be given by

$$\frac{\Delta C}{C} = \sqrt{\frac{2\tau}{T_{\text{traj}}}}, \quad (8)$$

where τ is the correlation time of the function and T_{traj} is the length of the trajectory. In the present paper, we generally fitted over a time interval of $[0, 4\tau - 5\tau]$.

III. RESULTS AND DISCUSSION

In this section, the wealth of information obtained from current QMD calculations is presented through figures and tables, and the general trends of the EOS as well as transport coefficients are detailed in the text. These transport coefficients are of interest not only to get insight into the interior physical properties of planets, but also to examine a series of theoretical models and experiments.

A. The equation of state

High precision EOS data of warm dense iron are essential for understanding the evolution of Earth and other applications as mentioned in the Introduction. Experimentally, the EOS of iron in the fluid regime has been studied through a gas gun, a chemical explosive, a nuclear explosive, and a high power laser.

TABLE I. Expansion coefficients A_{ij} for the internal energy E (eV/atom).

$A_{i,j}$	$j = 0$	$j = 1$	$j = 2$
$i = 0$	0.4131	0.4631	0.2292
$i = 1$	-0.9536	0.5606	-0.0154
$i = 2$	0.0772	-0.0188	0.0006

A crucial way to examine the EOS is the Hugoniot, which is the locus of points in (E, P, V) space satisfying the condition,

$$(E_0 - E_1) + \frac{1}{2}(V_0 - V_1)(P_0 + P_1) = 0, \quad (9)$$

where the subscripts 0 and 1 denote the initial and shocked states, respectively. This relation follows from conservation of mass, momentum, and energy for an isolated system compressed by a pusher at a constant velocity. In the canonical (NVT) ensemble in which both E and P are temperature dependent, the locus of states which satisfies Eq. (9) is the so-called principal Hugoniot, which describes the shock adiabat between the initial and the final states.

Wide-range EOS (densities from 12.5 to 25.0 g/cm³ and temperatures of 0.5–15 eV) has been calculated according to QMD simulations, and the internal energy E (eV/atom) and pressure P (GPa) are fitted by expansions in terms of density (g/cm³) and temperature (eV) as follows:

$$E = \sum A_{ij} \rho^i T^j, \quad (10)$$

$$P = \sum B_{ij} \rho^i T^j. \quad (11)$$

The fitted coefficients for $A_{i,j}$ and $B_{i,j}$ are summarized in Tables I and II. Here, the internal energy E and the pressure of the initial state at 7.85 g/cm³ and $T = 300$ K have been taken as zero.

The principal Hugoniot of iron has been shown in Fig. 1, and we compare the present results with previous theoretical and experimental data, such as a two-stage light gas gun [19], nuclear explosives [12–20], and a high intensity laser [21]. Theoretical results were obtained from VAAQP, INFERNO, the TF model, quantum Langevin molecular dynamics (QLMD), and the SESAME EOS tables [23–26,35]. Piron and Blenski [26] have used the VAAQP code and its options, such as the INFERNO option, and the TF option, so as to calculate electron contributions to the thermodynamic quantities. After adding an ion contribution to the pressure and internal energy, they obtain total quantities and calculate the Hugoniot shock adiabats. However, the interatomic contribution is not considered in these average atom (AA) models. The SESAME table [23] is composed of three terms: an electron contribution, an ion contribution, and a cold-curve contribution. It is worth noting

 TABLE II. Expansion coefficients B_{ij} for pressure P (GPa).

$B_{i,j}$	$j = 0$	$j = 1$	$j = 2$
$i = 0$	-16.0334	8.2077	-5.3060
$i = 1$	-48.3815	11.9455	0.3493
$i = 2$	5.4347	-0.22734	0.0015

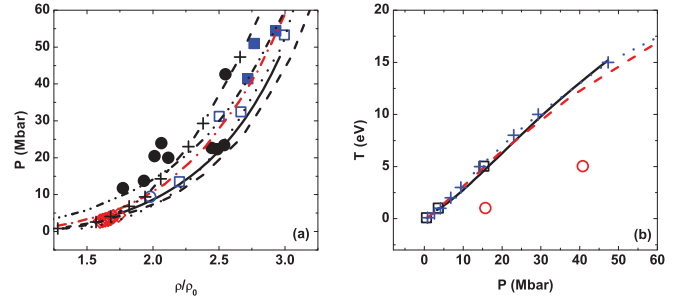


FIG. 1. (Color online) Equation of state for fluid iron. (a) Principal Hugoniot curve: results of the present paper (solid line) are compared with the SESAME-EOS table (dashed line) [23], INFERNO (dotted line) [26], the TF model (dashed-dot-dotted line) [26], VAAQP (dashed-dotted line) [26], and QLMD simulations (crosses) [35]. Experimental data by Brown and McQueen (open diamonds) [19], Krupnikov *et al.* (open circles) [15], Trunin and co-workers (solid squares) [16–18], Al'tshuler and co-workers (open squares) [12–14], and Batani *et al.* (solid circles) [21] are also plotted; (b) temperature along the Hugoniot: The present results (solid line) are shown with the results from previous QMD (open squares) [24,25], the TF model (open circles) [24,25], the SESAME table (dashed line) [24,25], and QLMD simulations (crosses) [35].

that the theoretical framework of constructing the SESAME-EOS table is not clearly defined. Moreover, the process of shifting the total pressure to fit the cold curve may lead to severe consequences in the EOS.

The present QMD simulation results are accordant with data from the gas gun [19] and nuclear experiments [12–20] but predict lower pressures compared with high intensity laser experiments [21] at ρ/ρ_0 from 1.75 to 2.5. This may be due to the preheating of samples in experiments and results in an unexpected higher pressure. The TF [26] model generally predicts highest pressures compared with other theoretical models at a certain density and temperature. Due to the presence of many-body interactions as well as collective quantum electronic distributions, QMD simulations provide more reliable predictions compared with the AA models (VAAQP and INFERNO) [26]. The SESAME table [23] only agrees with experiments at pressures below 5 Mbar. QLMD results [35] show accordance with our data at pressures below 10 Mbar, however, QLMD predicts a higher pressure compared with our simulations at $\rho/\rho_0 > 2$. Along the Hugoniot, we also examine the shock temperature, which is difficult to be determined experimentally, although theoretical simulations have been proved to be powerful tools for providing predictions. The present QMD simulation results agree well with previous QMD (see Refs. [24,25] and references therein) and QLMD [35] simulations [Fig. 1(b)]. The shock temperature obtained from the SESAME table and TF model [24,25] is lower compared with QMD results.

B. Diffusion and viscosity

QMD simulations have been used to study the dynamic properties of iron in the warm dense regime. A sample of the QMD results, together with their fits for the self-diffusion coefficient and viscosity at 20.0 g/cm³ with temperatures of

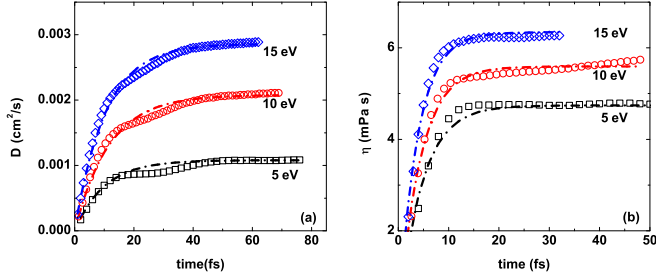


FIG. 2. (Color online) (a) Self-diffusion coefficient and (b) viscosity as functions of time at a density of 20.0 g/cm^3 and different temperatures of 5.0 (squares), 10.0 (circles), and 15.0 eV (diamonds). Their fits (dashed-dotted lines) are performed for a sample window of $[0, 4\tau]$ to 5τ .

5.0, 10.0, and 15.0 eV, are displayed in Fig. 2. The current simulations have a trajectory of 20–80 ps and correlation times between 200 and 400 fs. The computed error lies within 10% for the viscosity. The fitting procedure and extrapolation to infinite time will introduce a total uncertainty of $\sim 20\%$. Because the particle average gives an additional $\frac{1}{\sqrt{N}}$ advantage, the error in the self-diffusion coefficient is less than 1%.

In this paper, we intend to compare our results with an idealized model, namely, the one component plasma (OCP) model where ions move classically within a neutralizing background of electrons under the Coulomb potential. It has been demonstrated by Hansen *et al.* [36] and Bastea [37] that the transport coefficients, such as diffusion and viscosity, can be characterized by the ionic coupling parameter,

$$\Gamma = \frac{Z^2 e^2}{ak_B T}, \quad (12)$$

where Ze is the ion charge and $a = (3/4\pi n_i)^{1/3}$ is the ion-sphere radius with number density $n_i = \rho/M$. In fact, the OCP model is limited within a fully ionized plasma, and the determination of the ionization degree restricts the applications of the OCP formulas in the warm dense regime. Here, we choose $Z = 2$ (corresponding to a full ionization of 4s electrons in iron) in Eq. (12) to get OCP transport coefficients.

The results for self-diffusion coefficients at a sample density of 20.0 g/cm^3 have been shown in Fig. 3(a). Compared with QMD simulations, the OCP model [36] predicts a larger self-diffusion coefficient as well as the slope with respect to temperatures above 3 eV. The combined contribution from the interatomic potential and kinetic motion of particles will lead to a local minimum for the viscosity as shown in Fig. 3(b). The OCP model [37] indicates the local minimum around 2.5 eV, whereas, it is 5.0 eV, predicted by QMD simulations.

After obtaining the self-diffusion coefficient and viscosity in a self consistent way, we now turn to examine the Stokes-Einstein (SE) relation, which connects the diffusion and shear viscosity by

$$F_{SE}[D, \eta] = \frac{D\eta}{k_B T n_i^{1/3}} = C_{SE}, \quad (13)$$

where F_{SE} is a shorthand notation for the relationship between the transport coefficients and C_{SE} is a constant. C_{SE} was first

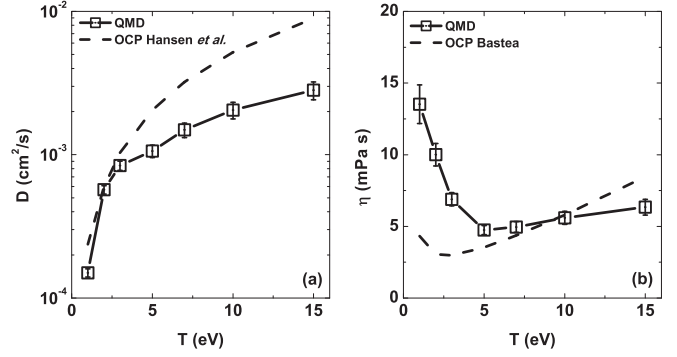


FIG. 3. (a) Self-diffusion coefficient and (b) viscosity as functions of temperature at a density of 20.0 g/cm^3 . The present QMD results are denoted by open squares, whereas, OCP data [36,37] are presented as dashed lines. Only the statistical error has been considered here.

derived based on the motion of a test particle through a solvent and was assumed to lie between $1/6\pi$ [38] and $1/4\pi$ [39] depending on the limits of the slip coefficient from infinity (stick) to zero (slip). Then, in 2006, Chisolm and Wallace [40] provided an empirical value of 0.18 ± 0.02 from a theory of liquids near melting. In this paper, we reexamine the SE relation with respect to QMD simulations as has been shown in Fig. 4 where QMD calculated C_{SE} is plotted with respect to $1/ak_B T$. Due to the fact that the diffusion coefficient increases almost linearly with respect to temperature and cancels the temperature dependence of the denominator in Eq. (13), as a consequence, C_{SE} is dominated by the high-pressure behavior of the viscosity. C_{SE} 's from QMD simulations are generally bounded by the classical values of C_{SE} from below (slip limit) and the Chisolm-Wallace liquid metal value as in Fig. 4. In the dynamic region explored, we do not observe any signs for

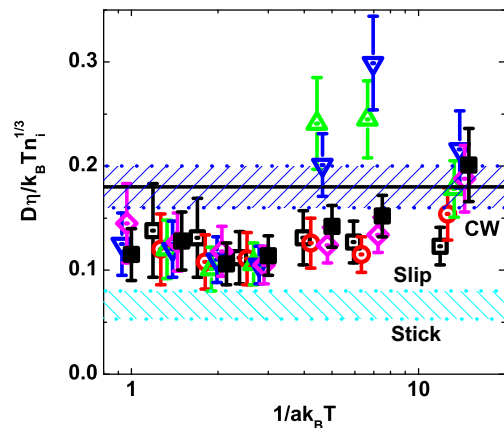


FIG. 4. (Color online) Examination of the Stokes-Einstein relation with respect to $1/ak_B T$ in the warm dense region. The present results at 12.5 (open squares), 15.0 (open circles), 17.5 (up-open triangles), 20.0 (down-open triangles), 22.5 (open diamonds), and 25.0 g/cm^3 (solid squares) are shown. Predictions by Chisolm and Wallace [40] are shown as the dotted blue region and are denoted as “CW” in the figure. The flat dashed cyan lines show the constant values of C_{SE} for stick and slip boundary conditions [38,39].

the change from potential to kinetics dominated regimes as in Be [41].

IV. CONCLUSION

To summarize, systematic QMD simulations have been performed to study iron in the warm dense regime for densities ranging from 12.5 to 25.0 g/cm³ and for temperatures from 0.5 to 15 eV. The present paper concentrated on the properties, such as the EOS, the diffusion coefficient, and the viscosity, which are of crucial interest in astrophysics and other applications. A wide-range EOS has been built by fitting the QMD data into a smooth function. The principal Hugoniot curve obtained from QMD simulations agrees well with nuclear

explosive experiments up to ~50 Mbar but is soft compared with the results from high power laser experiments, which can be attributed to the preheating of the samples. Comparison between the QMD transport coefficients and the OCP model is presented and is discussed. Classical models are examined by QMD simulations and have been found to hold the general features of the Stokes-Einstein relation in the warm dense region that we explored.

ACKNOWLEDGMENTS

This work was supported by the NSFC under Grants No. 11275032, No. 11005012, and No. 51071032, by the National Basic Security Research Program of China, and by the National High-Tech ICF Committee of China.

-
- [1] D. Andraut, S. Petitgirard, G. L. Nigro, J.-L. Devidal, G. Veronesi, G. Garbarino, and M. Mezouar, *Nature (London)* **487**, 354 (2012).
- [2] J. D. Lindl, P. Amendt, R. L. Berger, S. G. Glendinning, S. H. Glenzer, S. W. Haan, R. L. Kauffman, O. L. Landen, and L. J. Suter, *Phys. Plasmas* **11**, 339 (2004).
- [3] T. Auguste, F. de Gaufridy de Dortan, T. Ceccotti, J. F. Hergott, O. Sublemontier, D. Descamps, and M. Schmidt, *J. Appl. Phys.* **101**, 043302 (2007).
- [4] J. E. Bailey, G. A. Rochau, C. A. Iglesias, J. Abdallah, J. J. MacFarlane, I. Golovkin, P. Wang, R. C. Mancini, P. W. Lake, T. C. Moore, M. Bump, O. Garcia, and S. Mazevet, *Phys. Rev. Lett.* **99**, 265002 (2007).
- [5] L. B. Da Silva, B. J. MacGowan, D. R. Kania, B. A. Hammel, C. A. Back, E. Hsieh, R. Doyas, C. A. Iglesias, F. J. Rogers, and R. W. Lee, *Phys. Rev. Lett.* **69**, 438 (1992).
- [6] G. A. de Wijs, G. Kresse, L. Vočadlo, D. Dobson, D. Alfè, M. J. Gillan, and G. D. Price, *Nature (London)* **392**, 805 (1998).
- [7] D. Alfè, G. D. Price, and M. J. Gillan, *Phys. Rev. B* **65**, 165118 (2002).
- [8] W. J. Nellis, J. A. Moriarty, A. C. Mitchell, and N. C. Holmes, *J. Appl. Phys.* **82**, 2225 (1997).
- [9] W. B. Hubbard, W. J. Nellis, A. C. Mitchell, N. C. Holmes, S. S. Limaye, and P. C. Mccandless, *Science* **253**, 648 (1991).
- [10] J. M. Brown, J. N. Fritz, and R. S. Hixson, *J. Appl. Phys.* **88**, 5496 (2000).
- [11] R. Boehler, *Rev. Geophys.* **38**, 221 (2000).
- [12] L. V. Al'tshuler, A. A. Bakanova, I. P. Dudoladov, E. A. Dynin, R. F. Trunin, and B. S. Chekin, *J. Appl. Mech. Tech. Phys.* **22**, 145 (1981).
- [13] L. V. Al'tshuler, B. N. Moiseev, L. V. Popov, G. V. Simakov, and R. F. Trunin, *Sov. Phys. JETP* **27**, 420 (1968).
- [14] L. V. Al'tshuler, N. N. Kalitkin, L. V. Kuz'mina, and B. S. Chekin, *Sov. Phys. JETP* **45**, 167 (1977).
- [15] K. K. Krupnikov, A. A. Bakanova, M. I. Brazhnik, and R. F. Trunin, *Sov. Phys. Dokl.* **8**, 205 (1963).
- [16] R. F. Trunin, M. A. Podurets, G. V. Simakov, L. V. Popov, and B. N. Moiseev, *Sov. Phys. JETP* **35**, 550 (1972).
- [17] R. F. Trunin, M. A. Podurets, L. V. Popov, V. N. Zubarev, A. A. Bakanova, V. M. Ktitorov, A. G. Sevast'yanov, G. V. Simakov, and I. P. Dudoladov, *Sov. Phys. JETP* **75**, 777 (1992).
- [18] R. F. Trunin and G. V. Simakov, *J. Exp. Theor. Phys.* **76**, 1090 (1993).
- [19] J. M. Brown and R. G. McQueen, *J. Geophys. Res.* **91**, 7485 (1986).
- [20] *LASL Shock Hugoniot Data*, edited by S. P. Marsh (University of California Press, Berkeley, 1980).
- [21] D. Batani, A. Morelli, M. Tomasini, A. Benuzzi-Mounaix, F. Philippe, M. Koenig, B. Marchet, I. Masclat, M. Rabec, C. Reverdin, R. Cauble, P. Celliers, G. Collins, L. Da Silva, T. Hall, M. Moret, B. Sacchi, P. Baclet, and B. Cathala, *Phys. Rev. Lett.* **88**, 235502 (2002).
- [22] R. M. More, K. H. Warren, D. A. Young, and G. B. Zimmerman, *Phys. Fluids* **31**, 3059 (1998).
- [23] K. S. Holian, LANL Report No. LA-10160-MS UC-34, 1984 (unpublished).
- [24] F. Lambert, J. Clérouin, and G. Zérah, *Phys. Rev. E* **73**, 016403 (2006).
- [25] F. Lambert, J. Clérouin, and S. Mazevet, *Europhys. Lett.* **75**, 681 (2006).
- [26] R. Piron and T. Blenski, *Phys. Rev. E* **83**, 026403 (2011).
- [27] H. F. Wilson and B. Militzer, *Phys. Rev. Lett.* **108**, 111101 (2012).
- [28] R. M. Martin, *Electronic Structure: Basic Theory and Practical Methods* (Cambridge University Press, Cambridge, U.K., 2004).
- [29] G. Kresse and J. Hafner, *Phys. Rev. B* **47**, R558 (1993).
- [30] G. Kresse and J. Furthmüller, *Phys. Rev. B* **54**, 11169 (1996).
- [31] P. H. Hünenberger, *Adv. Polym. Sci.* **173**, 105 (2005); D. J. Evans and B. L. Holian, *J. Chem. Phys.* **83**, 4069 (1985).
- [32] M. P. Allen and D. J. Tildesley, *Computer Simulation of Liquids* (Oxford University Press, New York, 1987).
- [33] J. D. Kress, J. S. Cohen, D. P. Kilcrease, D. A. Horner, and L. A. Collins, *Phys. Rev. E* **83**, 026404 (2011).

- [34] R. Zwanzig and N. K. Ailawadi, *Phys. Rev.* **182**, 280 (1969).
- [35] J.-Y. Dai, D.-D. Kang, Z.-X. Zhao, Y.-Q. Wu, and J.-M. Yuan, *Phys. Rev. Lett.* **109**, 175701 (2012).
- [36] J. P. Hansen, I. R. McDonald, and E. L. Pollock, *Phys. Rev. A* **11**, 1025 (1975).
- [37] S. Bastea, *Phys. Rev. E* **71**, 056405 (2005).
- [38] A. Einstein, *Z. Elektrochem.* **14**, 235 (1908).
- [39] W. Sutherland, *Philos. Mag.* **9**, 781 (1905).
- [40] E. Chisolm and D. Wallace, in *Shock Compression of Condensed Matter*, edited by M. D. Furnish, M. Elert, T. P. Russell, and C. T. White, AIP Conf. Proc. No. 845 (AIP, New York, 2006), p. 53.
- [41] C. Wang, Y. Long, M.-F. Tian, X.-T. He, and P. Zhang, *Phys. Rev. E* **87**, 043105 (2013).